Hindawi
Complexity
Volume 2020, Article ID 8852186, 12 pages
https://doi.org/10.1155/2020/8852186

Research Article

Real-Time Optimal Control Strategy for Multienergy Complementary Microgrid System Based on Double-Layer Nondominated Sorting Genetic Algorithm

Min Mou, Yuhao Zhou, Wenguang Zheng, Zhongping Zhang, Da Lin, and Dongdong Ke

Huadian Electric Power Research Institute Co. Ltd, Hangzhou, Zhejiang 310013, China

Correspondence should be addressed to Min Mou; min-mou@chder.com

Received 22 August 2020; Revised 1 October 2020; Accepted 16 October 2020; Published 29 October 2020

Academic Editor: Zhile Yang

Because of the problems of low operation efficiency and poor energy management of multienergy input and output system with complex load demand and energy supply, this paper uses the double-layer nondominated sorting genetic algorithm to optimize the multienergy complementary microgrid system in real-time, allocating reasonably the output of each energy supply end and reducing the energy consumption of the system on the premise of meeting the demand of cooling, thermal and power load, so as to improve the economy of the whole system. According to the system load demand and operation mode, the first layer of this double-layer operation strategy calculates the power required by each node of the microgrid system to reduce the system loss. The second layer calculates the output of each equipment by using nondominated sorting genetic algorithm with various energy values calculated in the first layer as constraint conditions, considering the operation characteristics of various equipment and aiming at economy and environmental protection. In this paper, a typical model of energy input-output is established. This model combines with the operation control strategy suitable for multienergy complementary microgrid system, considers the operation mode and equipment characteristics of the system, and uses a double-layer nondominated sorting genetic algorithm to optimize the operation of each equipment in the multienergy complementary system in real time, so as to reduce the operation cost of the system.

1. Introduction

Multienergy complementary microgrid system is a multi-input and multi-output energy system, which generally covers integrated power supply, gas supply, heating supply, cold supply, and other energy systems as well as related communication and information infrastructure. The efficient economic and environmental protection operation of multienergy complementary system is the development direction of the energy industry in the future. For the energy efficiency to further be improved and the large-scale utilization of various new energy source's to be promoted, the deep integration and close interaction of multienergy sources, networks, and loads are the inevitable trend of future energy system development. Therefore, the research on multienergy complementary collaborative optimization has prospective and huge engineering application value [1].

Due to the differences in the development of different energy systems, the energy supply is often planned, designed, and operated independently, and there is a lack of coordination among them, which results in low energy utilization rate, weak overall security, and self-healing ability of energy supply system. The multienergy complementary system is a nonlinear system with the characteristics of equipment diversity, complex operation characteristics, and variable load; therefore, the problem of collaborative optimization is more important. The energy consumption mode of multienergy complementary microgrid system mainly includes three types, cooling, heating, and electricity; since the energy consumption side of the multienergy complementary microgrid system is not controllable, only by regulating and controlling the energy supplied by the

equipment at the energy supply side of the system, that is, the energy input end, can achieve the purpose of efficient and economic operation of the system.

At present, some researches have been done on the optimal energy allocation of multienergy complementary microgrid system at home and abroad, such as Jose L et al. considered the cost of system life cycle and pollutant emission as the objective equation to optimize the system [2]. Abbe S et al. considered three objectives at the same time to optimize the system; the methodology combined life cycle cost, embodied energy, and loss of power supply probability [3]. Diaf et al. studied the optimal sizing of stand-alone hybrid PV/wind system in Corsica Island based on technical-economic optimization [4]. Ding M. et al. established the scheduling model, which is based on three different operation strategies, to optimize operation scheduling through the environmental benefits of the two objectives [5]. Aghaei et al. developed a multiobjective self-scheduling optimization for CCHP (combined cooling, heating, and power system) based microgrid. The optimization considered minimizing the operational cost and emission [6]. Nwuluand Xia proposed the optimal dispatch strategy for hybrid PV/wind diesel system incorporated with the demand response program [7]. Some of these studies focus on static optimization of multienergy complementary system with cost or environment as the goal; some real-time optimization strategies are only for microgrid but do not optimize the control strategy of multienergy complementary system with cooling, heating, and power.

In this paper, a real-time optimal control strategy of multienergy complementary microgrid system based on double-layer nondominated sorting genetic algorithm is proposed to optimize the multienergy complementary microgrid system in real-time and reasonable distribute the output of each energy supply end [8, 9]. In this paper, a typical multienergy complementary microgrid system is studied. The structure of the multienergy complementary microgrid system is shown in Figure 1, which mainly includes wind turbine (WT), photovoltaic power generation (PV), internal combustion engine (GE), absorption chiller (AC), electric refrigerator (EC), electric boiler (EB), battery storage (BS), and cooling/heating storage (HS) equipment [10]. Firstly, the first layer of nondominated sorting genetic algorithm model is established to calculate the power demand of each node in the microgrid system to reduce the system loss by considering the operation mode and load demand of the system [11]. Secondly, the second layer uses the nondominated sorting genetic algorithm to calculate the output of each equipment through taking the calculation results of the first layer as the constraint, considering the operation characteristics of various equipment and taking the economy and environmental protection as the goal [12, 13]. Finally, the control strategy studied in this paper is applied to the multienergy complementary microgrid system in a certain area. The results of the example show that the performance, economy, reliability, and environmental protection of the multienergy complementary microgrid system are greatly improved by the double-layer nondominated sorting genetic algorithm.

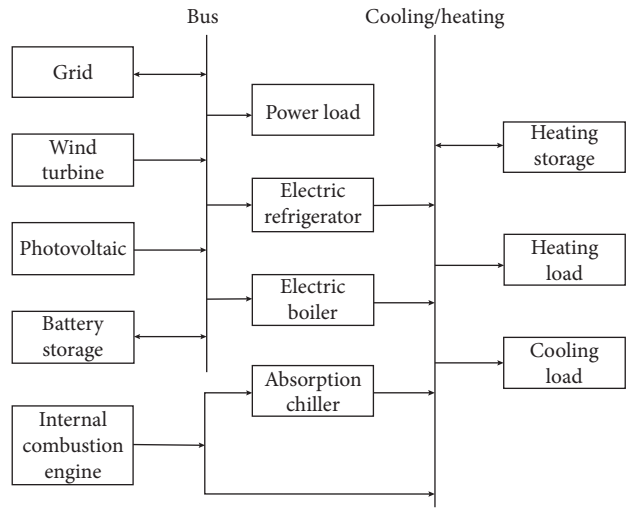

Figure 1: Multienergy complementary system structure.

2. Operation Strategy

The load demand and external environment resources in different time periods are different, and the priority of cooling and heating demand is also different. Therefore, the real-time operation control strategy of multienergy complementary microgrid system can improve the economy of the whole system.

Based on the characteristics of multienergy complementary microgrid system, this paper proposes two different operation strategies: power load priority and cooling and heating load priority, so as to optimize the operation mode of each equipment in the microgrid system.

2.1. Power Load Priority. In order to reduce the pollutant emission of the system, this strategy is that clean energy power generation is given priority, which gives priority to meet the power load demand of users. The operation principle is as follows:

(i) When the power load is lower than the total power generation of clean energy, clean energy such as wind power and solar energy is used to generate electricity; the surplus electricity is used to charge the electric energy storage, and the cooling and heating load demand is met by electric refrigeration.

(ii) When the power load is higher than the renewable energy generation capacity, the wind turbine and photovoltaic power supply directly to the power load, and the excess load is supplemented by electric energy storage discharge. At this time, the cooling load is met by electric refrigeration.

(iii) If the electric energy storage is at the minimum level or the discharge is not enough to supplement the electric load, the internal combustion engine is started to the rated power to generate electricity. The excess power is used to charge the electric energy storage. At this time, the cooling load is met by LiBr unit. If the cooling load's output power of lithium

bromide unit is insufficient, the additional cooling load can be supplemented by electric refrigeration. If the electric energy storage has reached the maximum state of charge, the internal combustion engine will start power tracking.

(iv) When the power load is higher than the renewable energy and internal combustion engine, the wind turbine of photovoltaic internal combustion engine directly supplies the power load, and the excess load is supplemented by electric energy storage discharge. The cooling load is met by LiBr unit. If the cooling load's output power of lithium bromide unit is insufficient, the additional cooling load can be supplemented by electric refrigeration.

2.2. Cooling and Heating Load Priority. This strategy gives priority to meet the user's cooling load demand and gives priority to the use of internal combustion engine for CCHP. The operation strategy is as follows:

(i) If the cooling load demand is less than the rated power of the absorption chiller and the renewable power generation resources are less, the internal combustion engine power will track the load for power generation, and the cooling load will be provided by the absorption refrigeration unit.

(ii) If the cooling load demand is less than the rated power of the absorption refrigeration unit and the renewable power generation resources are larger, the cooling load is provided by the absorption refrigeration unit and the electric refrigeration.

(iii) If the cooling load demand is larger than the rated power of absorption refrigeration unit, the internal combustion engine runs at full power, and the insufficient cooling load is provided by electric refrigeration. If the power generated by the internal combustion engine is larger than the electric load, the excess power will charge the electric energy storage.

Under this operation strategy, the charge and the discharge of energy storage are the same as those in scheme *i*.

3. Multiobjective Nondominated Sorting Genetic Algorithm

3.1. Mathematical Description of Multiobjective Optimization Algorithm. Taking the minimization multiobjective problem with constraints as an example, the multiobjective optimization problem can be described as follows:

$$\begin{cases} \min f(X) = [f_1(X), f_2(X) \dots f_n(X)], \\ \text{s.t. } g_i(X) \le 0, \quad i = 1, 2, 3 \dots, \\ h_j(X) = 0, \quad j = 1, 2, 3 \dots, \end{cases} \tag{1}$$

where $f(X)$ denotes a vector space with n objective functions, $g_i(X)$ denotes the i^{th} inequality constrained function, $h_j(X)$ denotes the j^{th} equality constraint, and $X = (x_1, x_2, \dots, x_m)$ denotes a vector space with m decision variables [14].

3.2. Decision-Making in Multiobjective Optimization. It is a series of discrete solutions obtained by multiobjective nondominated sorting genetic algorithm. How to choose an optimal scheme among these discrete points is the key to multiobjective optimization. In this paper, a method of selecting the optimal scheme based on geometric distance method is proposed, the central idea is that the geometric distance between the optimal scheme and the positive ideal scheme is the shortest, while the geometric distance between the optimal scheme and the reverse ideal scheme is the longest. The optimal scheme comes from the optimized Pareto frontier, positive ideal solution refers to the scheme that can optimal satisfy every objective function at the same time, and negative ideal solution refers to the scheme that does not optimal satisfy any objective function.

The calculation of spatial/geometric distance (d_i^+) of any scheme i from Pareto frontier to positive ideal solution is as follows:

$$d_i^+ = \sqrt{\sum_{j=1}^{m} \left(S_{ij} - S_j^{p-\text{ideal}}\right)^2}, \tag{2}$$

where m denotes the number of objective functions, j denotes the dimension, and $S_{ij} - S_j^{p-\text{ideal}}$ denotes the straight line distance from scheme i to the j dimension of positive ideal solution。

The calculation of spatial/geometric distance (d_i^+) of any scheme i from Pareto frontier to negative ideal solution is as follows:

$$d_i^- = \sqrt{\sum_{j=1}^{m} \left(S_{ij} - S_j^{n-\text{ideal}}\right)^2}, \tag{3}$$

where $m S_{ij} - S_j^{n-\text{ideal}}$ denotes the straight distance from scheme i to the j dimension of negative ideal solution.

The coefficients ω_i defined below are as follows:

$$\omega_i = \frac{d_i^+}{d_i^+ + d_i^-}, \tag{4}$$

Through the formulae (2)–(4), any scheme of ω_i from Pareto frontier can be calculated, then the scheme in which minimum ω_i is corresponded is the final optimal solution.

4. Mathematic Model for Multienergy System

The multienergy complementary distributed energy system is the expansion of traditional distributed energy application and is the physical concept of integration [15]. It integrates multiple energy technologies to realize the collaborative optimization of multienergy sources. The multienergy complementary distributed energy system has a variety of energy resources input, but it is not a simple superposition of multiple energy sources. It uses the energy of different grades in a systematic way comprehensively and complementarily uses the energy of the system and makes overall arrangements for the coordination and conversion of various energies, so as

to achieve the most reasonable effect and benefit of energy utilization. The structure of the multienergy complementary system generally includes wind power, photovoltaic, internal combustion engine, absorption chiller, waste heat boiler, battery storage, heating storage, and ice storage.

4.1. Wind Power. This paper mainly considers variable speed constant frequency wind power generation, whose output power expression is closely related to the operation mode of wind turbine [16]. According to the working principle of the wind turbine, when the wind speed is less than the cut-in wind speed, the wind turbine does not generate electricity, when the wind speed is larger than the cut-in wind speed and less than the rated wind speed, the wind turbine generates electricity,\ and the output power changes with the wind speed, when the wind speed is larger than the rated wind speed and less than the cut-out wind speed, the wind turbine outputs the rated power, and when the wind speed is larger than the cut-out wind speed, the wind turbine stops working and does not generate electricity. The output of wind turbine at time t $P_{\mathrm{wt}}(\mathrm{t})$ is as follows:

$$\mathrm{P}_{\mathrm{wt}}(t)=\begin{cases}\mathrm{P}_{\mathrm{wt}}(t)=0, & V<V_{\mathrm{ci}},\\ \mathrm{P}_{\mathrm{wt}}(t)=aV^{3}-bP_{\mathrm{r}}, & V_{\mathrm{ci}}<V<V_{\mathrm{r}},\\ \mathrm{P}_{\mathrm{wt}}(t)=P_{\mathrm{r}}, & V_{\mathrm{r}}<V<V_{\mathrm{co}},\\ \mathrm{P}_{\mathrm{wt}}(t)=0, & V_{\mathrm{co}}<V,\end{cases} \tag{5}$$

where $a=P_{\mathrm{r}}/(V_{\mathrm{r}}^{3}-V_{\mathrm{ci}}^{3})$, $b=V_{\mathrm{ci}}^{3}/(V_{\mathrm{r}}^{3}-V_{\mathrm{ci}}^{3})$, V_{ci} denotes the cut-in wind velocity, V_{co} is the cut-out wind velocity, V_{r} denotes the rated wind speed, and P_{r} denotes the rated power.

4.2. Photovoltaic. The output power of silicon solar cell module is related to many factors, including temperature and solar radiation intensity on the photovoltaic panel [17]. The photovoltaic power expressions in this paper that is expressed by the optimal operating point voltage and the optimal operating point current are as follows:

$$\begin{aligned}
&P_{\mathrm{pv}}(t)=I_{\mathrm{pv}}(t)V_{\mathrm{pv}}(t),\\
&I_{\mathrm{pv}}(t)=I_{\mathrm{sc}}\left(1-C_{1}\left(\exp\left(\frac{V_{\mathrm{pv}}-\Delta V}{C_{2}V_{\mathrm{oc}}}\right)-1\right)\right)+\Delta I,\\
&V_{\mathrm{pv}}(t)=V_{\mathrm{mp}}\left(1+0.0539\cdot\log\left(\frac{G_{t}}{1000}\right)\right)+\beta\Delta T,\\
&\Delta I=\alpha\left(\frac{G_{\mathrm{t}}}{G_{\mathrm{ref}}}\right)\Delta T+\left(\frac{G_{\mathrm{t}}}{G_{\mathrm{ref}}}-1\right)I_{\mathrm{sc}},\\
&\Delta T=T_{\mathrm{a}}-T_{\mathrm{ref}},\\
&\Delta V=V_{\mathrm{pv}}-V_{\mathrm{mp}},\\
&C_{1}=\left(1-\frac{I_{\mathrm{mp}}}{I_{\mathrm{SC}}}\right)\exp\left[\frac{-V_{\mathrm{mp}}}{C_{2}V_{\mathrm{OC}}}\right],\\
&C_{2}=\frac{\left(V_{\mathrm{mp}}/V_{\mathrm{OC}}\right)-1}{\ln\left(1-\left(I_{\mathrm{mp}}/I_{\mathrm{SC}}\right)\right)},
\end{aligned} \tag{6}$$

where I_{pv} denotes the optimum operating current, V_{pv} denotes the optimum operating voltage, I_{sc} denotes the short circuit current, I_{mp} denotes the maximum power point current, V_{mp} denotes the maximum power point voltage, V_{OC} denotes the open circuit voltage, α denotes the temperature coefficient for current, β denotes the temperature coefficient for voltage, G_t denotes the tilted solar irradiation on PV panel, $G_{\mathrm{ref}}=1000\,\mathrm{W/m^2}$ is the reference solar irradiation, T_a denotes the ambient temperature that changes over time, $T_{\mathrm{ref}}=25^{\circ}\mathrm{C}$ is the reference battery temperature, and ΔI, ΔV, and ΔT are the modified current, modified voltage, and modified temperature, respectively.

4.3. Internal Combustion Engine. The internal combustion engine consumes natural gas for power generation, and the waste heat generated can be used for refrigeration of absorption refrigeration units. The internal combustion engine can supply power load and meet the user's demand for cooling and heating load at the same time. The heating power output of the internal combustion engine at time $tQ_{\mathrm{GE.heat}}(t)$ is as follows:

$$Q_{\mathrm{GE.heat}}(t)=P_{\mathrm{GE}}(t)\left(\frac{1-\eta_{\mathrm{GE}}(t)}{\eta_{\mathrm{GE}}(t)}\right), \tag{7}$$

where $P_{\mathrm{GE}}(t)$ denotes the real-time rate of work of the internal combustion engine and $\eta_{\mathrm{GE}}(t)$ denotes the real-time efficiency of internal combustion engines. The efficiency of internal combustion engine is related to its real-time load [18].

The fuel consumption of internal combustion engine at time t is as follows:

$$V_{\mathrm{GE}}(t)=\sum\frac{P_{\mathrm{GE}}(t)\Delta t}{\eta_{\mathrm{gas}}\eta_{\mathrm{GE}}(t)\mathrm{LHV}}, \tag{8}$$

where η_{gas} denotes the natural gas utilization rate of internal combustion engine and $\mathrm{LHV}=36.82\,\mathrm{MJ/m^3N}$ denotes the low calorific value of natural gas.

4.4. Absorption Chiller. Absorption chiller unit is a kind of refrigerator driven by heat energy. Its heat energy is the use of exhaust heat of internal combustion engine. Then, the cooling capacity at time t $(Q_{\mathrm{AC.cool}}(t))$ is expressed as follows:

$$Q_{\mathrm{AC.cool}}(t)=Q_{\mathrm{AC.heat}}(t)\mathrm{COP}_{\mathrm{AC}}, \tag{9}$$

where $Q_{\mathrm{AC.heat}}(t)$ denotes the heating power absorbed by absorption chiller and $\mathrm{COP}_{\mathrm{AC}}$ denotes the energy efficiency coefficient of absorption chiller unit and is related to the load rate of absorption chiller unit.

4.5. Electric Refrigerating Machine. Electric refrigerator is a kind of refrigerator driven by electric energy. Since the refrigerating capacity of absorption refrigeration unit is limited by the residual heat of internal combustion engine, while the electric refrigeration unit is not constrained, it can effectively supplement the cooling capacity required by users

in time; the expression of cooling capacity at t time $(Q_{EC(t)})$ is as follows:

$$Q_{EC(t)} = P_{EC}(t)COP_{EC}, \tag{10}$$

where $P_{EC}(t)$ denotes the real-time power consumption of electric refrigeration and COP_{EC} denotes the energy efficiency coefficient of electric refrigeration and also related to the unit load rate.

4.6. Electric Boiler. Electric boiler is a kind of boiler equipment which takes electric power as energy and converts it into heat energy, then outputs the steam, high temperature water, or organic heat carrier with certain thermal energy. The expression of thermal output at time t is as follows:

$$Q_{EB(t)} = P_{EB}(t)COP_{EB}, \tag{11}$$

where $P_{EB}(t)$ denotes the real-time power consumption of electric thermal and COP_{EB} denotes the energy efficiency coefficient of electric heat and also related to the unit load rate.

4.7. Electric Energy Storage. The output power of battery is closely related to the operation state of the system, and there are many kinds of batteries. This paper assumes that the state of lead-acid battery at time t is related to that at time $t - \Delta t$ [19]. In this paper, the energy storage capacity of the battery is considered, and the real-time capacity $(C_{BS}(t))$ is shown as follows:

$$C_{BS}(t+1) = C_{BS}(t)(1-\sigma) - \left[P_{BS.cha}(t)\eta_{cha} - \frac{P_{BS.discha}(t)}{\eta_{discha}}\right]\Delta t, \tag{12}$$

where $P_{BS.cha}$ and $P_{BS.discha}$ are the charging and discharging powers of equipment, respectively, η_{cha} and η_{discha} are the charging and discharging efficiencies of equipment, respectively, and σ denotes the self-discharge rate of battery per hour.

4.8. Thermal Energy Storage. In the same way as electric energy storage equipment, the real-time capacity of thermal energy storage equipment $(C_{HS}(t))$ is as follows:

$$C_{HS}(t+1) = C_{HS}(t)(1-\tau) - \left[Q_{HS.cha}(t)\delta_{cha} - \frac{Q_{HS.discha}(t)}{\delta_{discha}}\right]\Delta t, \tag{13}$$

where $Q_{HS.cha}$ and $Q_{HS.discha}$ are the endothermic power and exothermic power of equipment, respectively, δ_{cha} and δ_{discha} are the thermal absorption efficiency and thermal release efficiency of thermal storage equipment, respectively, and τ denotes the self-loss rate of thermal storage equipment.

5. Double-Layer Multiobjective Optimization Algorithm

According to the system load demand and operation mode, the first layer of this two-layer operation strategy calculates the power required by each node of the microgrid system to reduce the system loss and the second layer calculates the output of each equipment by using nondominated sorting genetic algorithm with various energy values calculated in the first layer as constraint conditions, considering the operation characteristics of various equipment and aiming at economy and environmental protection.

5.1. First-Layer Optimization Algorithm. In the multienergy complementary microgrid system, the load and the operation state of each equipment change at any time. Reasonable energy allocation can effectively improve the operation performance of the system and improve the economic efficiency of the system. Therefore, the decision variables of the first layer are the demand capacity value of each node distributed generation [20].

According to the grid structure and power demand, reasonable configuration of DG capacity of each node can meet the energy demand of users and reduce the energy loss of the multienergy complementary microgrid system [21, 22]. Therefore, the objective of the first layer optimization algorithm is to minimize the power loss of microgrid system, and its objective function is as follows:

$$\begin{cases} \min P_{loss} = \sum_{k=1}^{N_1} G_{k(i,j)}\left(U_i^2 + U_j^2 - 2U_iU_j\cos\delta_{ij}\right), \\ \min \Delta U = \sum_{i=1}^{N_d}\left(\frac{U_i - U_i^{spec}}{\Delta U_i^{max}}\right)^2, \end{cases} \tag{14}$$

where P_{loss} denotes the active loss of power of multi-energy network, ΔU denotes the offset of load node voltage in multienergy network, N_1 denotes the number of branches in multienergy network, N_d denotes the number of nodes in multienergy network, $G_{k(i,j)}$ denotes the conductance of branch (i, j) is the number of the nodes at both ends of branch k, U_i and U_j are the voltage amplitude of nodes i and j, respectively, δ_{ij} denotes the phase angle difference of nodes i and j, U_i^{spec} denotes the expected voltage value of node i, and ΔU_i^{max} denotes the maximum allowable voltage deviation of node i, so $\Delta U_i^{max} = U_i^{max} - U_i^{min}$.

The energy transfer of multienergy complementary microgrid system is limited by the energy conservation of the network and the transmission capacity of the pipe network [23]. Therefore, the power constraints in the system are as follows.

5.1.1. Power Balance Constraints

$$\begin{cases} P_{Gi}(t) + P_{\mathrm{DG}i}(t) - P_{Li}(t) - U_i(t)\sum_{j=1}^{N_d} U_j(t)\left(G_{ij}\cos\delta_{ij} + B_{ij}\sin\delta_{ij}\right) = 0, \\ Q_{Gi}(t) - Q_{Li}(t) - U_i(t)\sum_{j=1}^{N_d} U_j(t)\left(G_{ij}\sin\delta_{ij} + B_{ij}\cos\delta_{ij}\right) = 0, \end{cases} \tag{15}$$

where P_{Gi}, P_{DGi}, and P_{Li} are the active power of the generator, distributed generation, and load of node i, respectively, G_{ij} andB_{ij} are the conductance and susceptance between nodes i and j, respectively, and Q_{Gi} and Q_{Li} are the reactive power of the generator and load of node i, respectively.

5.1.2. System Inequality Constraints

(1) Node voltage constraint:

$$V_{i\min} \le V_i(t) \le V_{i\max}, \quad i = 1, 2, \ldots, N_d, \tag{16}$$

where $V_{i\min}$ and $V_{i\max}$ are the voltage upper and lower limits of the i^{th} node, respectively.

(2) Upper limit constraint of DG active power:

$$0 \le P_{\mathrm{DG}i}(t) \le P_{\mathrm{DGmax}}, \quad i = 1, 2, \ldots, N_{\mathrm{DG}}, \tag{17}$$

where P_{DGmax} denotes the upper limit of DG active power and N_{DG} denotes the number of nodes which can be installed in DG.

(3) Branch transmission power constraint:

$$\left|P_k(t)\right| \le P_{k\max}, \quad k = 1, 2, \ldots, N_1, \tag{18}$$

where $P_{k\max}$ denotes the upper limit of transmission power of the k^{th} branch.

5.2. Second Layer Optimization Algorithm. Based on the results of the first layer optimization algorithm and real-time and reasonable configuration of the cooling, heating, and power output values of each equipment in the multienergy complementary microgrid system can improve the system operation economy and environmental protection [24], so the real-time output of each equipment is the decision variable of the optimization algorithm in this layer [25, 26].

The objective of this layer optimization algorithm is to optimize the economy and environmental protection, so the objective function is as follows:

$$\begin{cases} \min C_{\mathrm{total}} = C_{\mathrm{mainenance}} + C_{\mathrm{operation}}, \\ \min \mathrm{EM}_{\mathrm{plt}} = \sum_{i=1}^{n} P_{\mathrm{GE}}(t) \cdot (\alpha_i \cdot Q_i), \end{cases} \tag{19}$$

where C_{total} denotes the total cost of system operation, $C_{\mathrm{mainenance}}$ denotes the maintenance cost of system equipment, $C_{\mathrm{operation}}$ denotes the operation cost of system equipment, it mainly includes system electricity purchase cost and natural gas purchase cost, $\mathrm{EM}_{\mathrm{plt}}$ denotes the environmental cost of power generation, α_i denotes the i^{th} pollutant emission per unit power of internal combustion engine, Q_i denotes treatment fee for unit power of the i^{th} pollutant emission, and $P_{GE}(t)$ denotes the real-time electric power output by the internal combustion engine [27].

Equipment maintenance costs are as follows:

$$C_{\mathrm{mainenance}} = \sum u_{\mathrm{type}} \cdot P_{\mathrm{type}}(t) \cdot \Delta t, \tag{20}$$

where type = WT, PV, GE, BS, AC, EC, EB, HS, u_{type} denotes the maintenance factor of each equipment, and $P_{\mathrm{type}}(t)$ denotes the electric power of each equipment at time t.

Equipment operation costs are as follows:

$$C_{\mathrm{operation}} = P_{\mathrm{grid}}(t) \cdot \mathrm{Ct}_{\mathrm{ele}}(t) \cdot \Delta t + V_{\mathrm{GE}}(t) \cdot Ct_{\mathrm{gas}}(t) \cdot \Delta t, \tag{21}$$

where $P_{\mathrm{grid}}(t)$ denotes the power purchased from the grid for the system, $\mathrm{Ct}_{\mathrm{ele}}(t)$ denotes the real-time price of power grid, $V_{\mathrm{GE}}(t)$ denotes the volume of natural gas consumed by the system, and $\mathrm{Ct}_{\mathrm{gas}}(t)$ denotes the real-time price of natural gas (0.36 \$/m^3).

The constraints of the optimization algorithm in this layer mainly include system constraints, technical constraints, and operation constraints.

System constraints mainly limit the upper and lower limits of each equipment capacity of the system, and this part of the constraint is expressed as follows:

$$\begin{cases} P_{\mathrm{WT\_min}} \le P_{\mathrm{WT}}(t) \le P_{\mathrm{WT\_max}}, \\ P_{\mathrm{PV\_min}} \le P_{\mathrm{PV}}(t) \le P_{\mathrm{PV\_max}}, \\ P_{\mathrm{GE\_min}} \le P_{\mathrm{GE}}(t) \le P_{\mathrm{GE\_max}}, \\ P_{\mathrm{BS\_min}} \le P_{\mathrm{BS}}(t) \le P_{\mathrm{BS\_max}}, \\ P_{\mathrm{EC\_min}} \le P_{\mathrm{EC}}(t) \le P_{\mathrm{EC\_max}}. \end{cases} \tag{22}$$

When the operation strategy is power load priority, $P_{\mathrm{GS}} = P_{\mathrm{GS\_min}}$. When the operation strategy is cooling load priority, $P_{\mathrm{GS\_min}}$ needs to be set to meet 70% of maximum cooling load.

Technical constraints mainly include the technical limitation of equipment operation. When the internal combustion engine is running under variable conditions, the ramp rate constraint should also be met, which is as follows:

$$\begin{cases} P_{\mathrm{GE}}(t) - P_{\mathrm{GE}}(t-\Delta t) \le \Delta P_U, \\ P_{\mathrm{GE}}(t) - P_{\mathrm{GE}}(t-\Delta t) \le \Delta P_D, \end{cases} \tag{23}$$

where ΔP_U denotes the rate of rise limit and ΔP_D denotes the rate of descent limit.

The charge and discharge of electric energy storage should meet the following constraints:

$$\begin{cases} P_{\mathrm{BS.cha\_min}} \le P_{\mathrm{BS.cha}}(t) \le P_{\mathrm{BS.cha\_max}}, \\ P_{\mathrm{BS.discha\_min}} \le P_{\mathrm{BS.discha}}(t) \le P_{\mathrm{BS.discha\_max}}, \end{cases} \tag{24}$$

$P_{\mathrm{BS.cha\_min}}$ and $P_{\mathrm{BS.cha\_max}}$ are the maximum and minimum charging power of energy storage equipment, respectively, and $P_{\mathrm{BS.discha\_min}}$ and $P_{\mathrm{BS.discha\_max}}$ are the maximum and minimum discharge power of energy storage equipment, respectively. Furthermore, the battery capacity should also meet the following constraints: $\mathrm{SOC}_{\min} \le C_{\mathrm{bs}}(t) \le \mathrm{SOC}_{\max}$. $\mathrm{SOC}_{\min}$ and $\mathrm{SOC}_{\max}$ are the maximum and minimum storage capacity of power storage equipment, respectively.

Operation constraints mainly refer to the energy exchange constraints and the system energy conservation constraint between the multienergy complementary microgrid system and the power grid system, which are expressed as follows.

5.2.1. Energy Exchange Constraints. Energy exchange constraints are as follows:

$$\begin{cases} P_{\mathrm{WT}}(t) + P_{\mathrm{PV}}(t) + P_{\mathrm{GE}}(t) + P_{\mathrm{BS}}(t) - P_{\mathrm{EC}}(t) - P_{\mathrm{EB}}(t) - P_{\mathrm{EL}}(t) \le P_{\mathrm{ongrid\_max}}, \\ P_{\mathrm{EC}}(t) + P_{\mathrm{EB}}(t) + P_{\mathrm{EL}}(t) - P_{\mathrm{WT}}(t) - P_{\mathrm{PV}}(t) - P_{\mathrm{GE}}(t) - P_{\mathrm{BS}}(t) \le P_{\mathrm{grid\_max}}, \end{cases} \tag{25}$$

where $P_{\mathrm{EL}}(t)$ denotes the real-time power of total electric load of the system, $P_{\mathrm{ongrid\_max}}$ denotes the maximum value of the energy that the system can be connected to the grid, and $P_{\mathrm{grid\_max}}$ denotes the maximum amount of electricity the system can purchase from the grid.

5.2.2. Energy Conservation Constraint

Power balance constraint is shown as follows:

$$P_{\mathrm{WT}}(t) + P_{\mathrm{PV}}(t) + P_{\mathrm{GE}}(t) + P_{\mathrm{BS}}(t) + P_{\mathrm{grid}}(t) = P_{\mathrm{EC}}(t) - P_{\mathrm{EB}}(t) - P_{\mathrm{EL}}(t), \tag{26}$$

Heating power balance constraint is shown as follows:

$$Q_{\mathrm{GE.heat}}(t) + Q_{\mathrm{EB(t)}} + C_{\mathrm{HS}}(t) = Q_{\mathrm{AC.heat}}(t) + Q_{\mathrm{L.heat}}(t), \tag{27}$$

where $Q_{\mathrm{L.heat}}(t)$ denotes the heating load of the system at time t.

Cooling power balance constraint is shown as follows:

$$Q_{\mathrm{AC.cool}}(t) + Q_{\mathrm{EC}}(t) = Q_{\mathrm{L.cool}}(t), \tag{28}$$

where $Q_{\mathrm{L.cool}}(t)$ denotes the cooling load of the system at time t.

6. Case Study

6.1. Basic Data. This paper takes the architecture and load data of a regional multi-energy complementary microgrid system as an example to verify the effectiveness of the algorithm. The grid structure of the system is shown in Figure 2, the grid parameters (per unit value) are shown in Table 1, and the electrical load data of each node of the system are shown in Figures 3 and 4 (the reference capacity is 1 mW). This multienergy complementary microgrid system uses the optimization strategy based on double-layer nondominated sorting genetic algorithm to control the cooling, thermal, and power output of each equipment in the system in real-time. The economy and environmental protection of the system with and without this algorithm are compared and analyzed (assuming that the cooling, heating, and power load of the system remains unchanged and the meteorological parameters remain unchanged within one hour of the evaluation period).

In this paper, the first-layer optimization algorithm calculates the distributed generation capacity required by each node based on the grid structure and power load demand of multienergy complementary microgrid system. The second layer optimization algorithm calculates the output value of each equipment in the system through combining the results of the first layer algorithm, considering the cooling and thermal load demand of the system and the characteristics of each equipment. The parameters of wind turbine, photovoltaic and electric energy storage used in this system are shown in Tables 2–4.

The power ramp rate ΔP_U = 500 kW/h, the power ramp down rate ΔP_D = 650 kW/h, and the minimum operating power $P_{\min}$ = 130 kWof internal combustion engine in the system are shown in Table 5. Cop characteristic data of absorption chiller, electric refrigerator, and electric boiler used in the system are shown in Tables 6 and 7, respectively. The cooling and thermal load data, meteorological data, and real-time electricity price of the system on a certain day are shown in Figures 5–9. The power interaction between the multienergy complementary microgrid system and the power grid should meet the following requirements: $P_{\mathrm{ongrid\_max}}$ = 20 kW and $P_{\mathrm{grid\_max}}$ = 100 kW.

The population size of the two-layer optimization algorithm in this paper is 200, and the number of iterations is 100. The result of the first layer optimization algorithm is

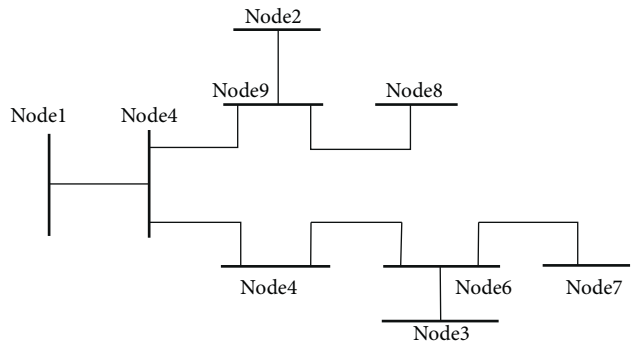

Figure 2: Topology of multienergy complementary microgrid system.

Table 1: Line parameter.

Initial points of line	End of line	Resistance	Inductance	Capacitance
1	4	0.000	0.025	0.000
4	5	0.007	0.040	0.017
5	6	0.016	0.073	0.039
3	6	0.000	0.025	0.000
6	7	0.005	0.043	0.023
9	2	0.000	0.027	0.000
8	9	0.014	0.070	0.033
9	4	0.004	0.037	0.019

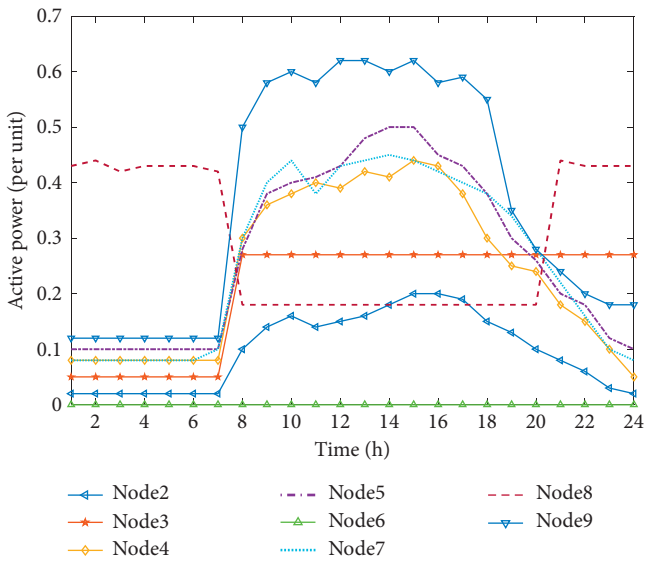

Figure 3: Active power data of load at each node.

that the node 8 needs 825 kW of electricity and the node 9 needs 713 kW. The maintenance cost of each equipment in the system is shown in Table 8, and the maintenance fee of pollutant emission t is shown in Table 9.

In this paper, different operation modes are used to optimize this example in real time based on double-layer nondominated sorting genetic algorithm. The results of power load priority operation are shown in Figure 9, and the results

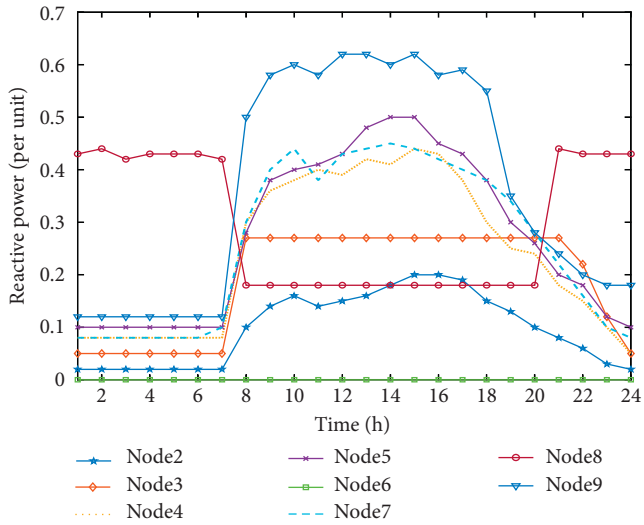

Figure 4: Reactive power data of load at each node.

Table 2: Wind generator parameter.

P_r (kW)	V_{in} (m/s)	V_r (m/s)	V_{out} (m/s)	N_{wind}^{max}
500	3	12	25	8

Table 3: Photovoltaic parameter.

P_r(kW)	V_{OC} (V)	I_{sc} (A)	V_{mp} (V)	I_{mp} (A)	Series number	Parallel number
100	64.6	6.14	54.7	5.76	5	64

Table 4: Battery storage parameter.

(%)σ	SOC_{max} (kWh)	SOC_{min} (kWh)	η_{cha}	$\eta_{dischar}$	$P_{BS.cha}$(C)	$P_{BS.discha}$(C)
98	20	2.5	90%	98%	0.3	3

Table 5: Internal combustion generation parameter.

Power	325 kW (%)	243.75 kW (%)	162.5 kW (%)
Load rate (L_r)	100	75	50
Efficiency (η)	41.6	39.7	35.7

Table 6: Absorption chiller parameter.

Cooling capacity	520 kW	390 kW	260 kW	130 kW
Load rate (L_r)	100%	75%	50%	25%
COP_{AC}	1.42	1.638	1.692	1.372

Table 7: Centrifugal chiller parameter.

Cooling capacity	500 kW	400 kW	300 kW	200 kW	100 kW
Load rate (L_r)	100%	80%	60%	40%	20%
COP_{EC}	5.75	6.04	6.09	5.29	3.45

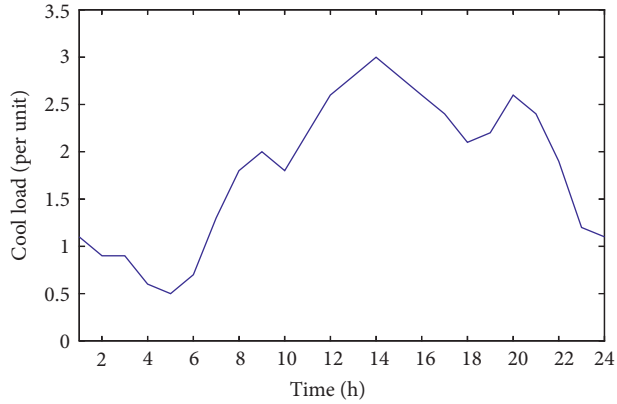

Figure 5: Cooling load data.

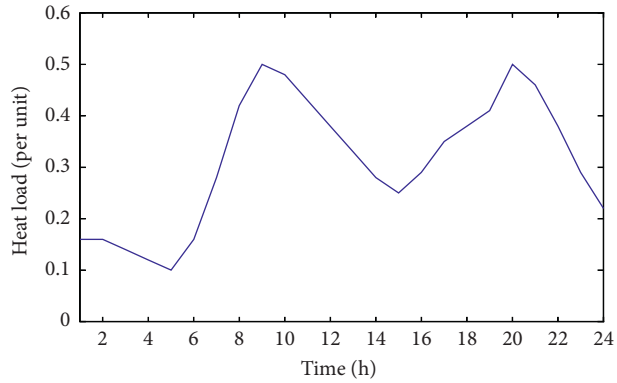

Figure 6: Thermal load data.

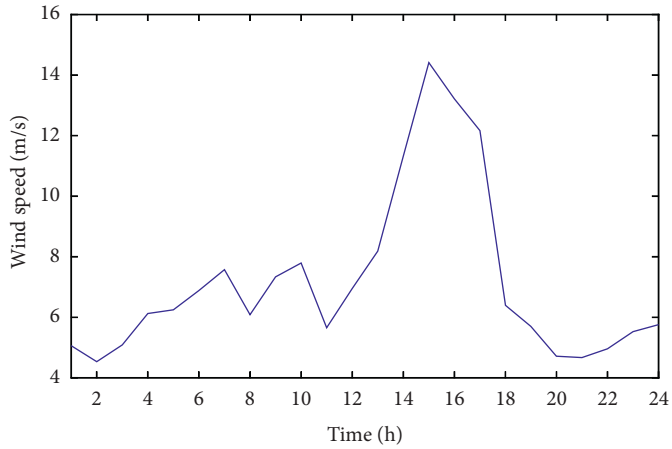

Figure 7: Wind resource data.

of cooling and thermal load priority operation are shown in Figures 10 and 11. The comparison of various indexes before and after optimization is shown in Tables 10 and 11.

The results show that the active power loss and voltage deviation of the multienergy complementary microgrid system are reduced by 51.41% and 41.89%, respectively, after using the real-time optimal control strategy based on double-layer nondominated sorting genetic algorithm. The total operation cost and pollutant emission control cost of the multienergy complementary microgrid system are reduced by 9.37% and 20.81%, respectively, when the power load priority operation mode is used; when the cooling and

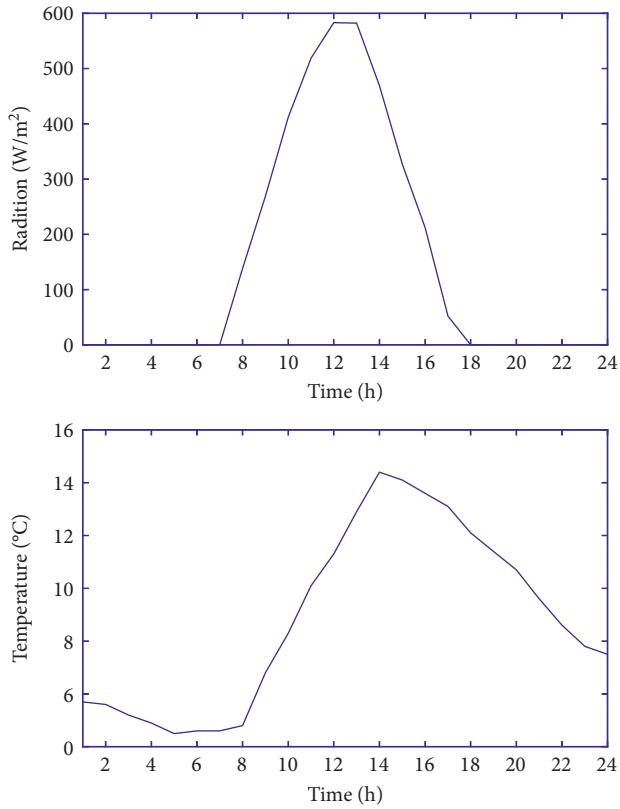

Figure 8: Solar resource data.

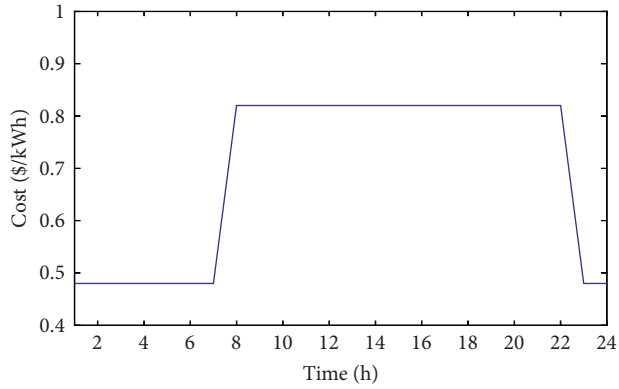

Figure 9: Real-time price of electricity.

Table 8: Equipment maintenance fee.

	WT	PV	GE	AC	EC	EB	BS	HS
Maintenance cost ($/kWh)	0.0296	0.0096	0.069	0.032	0.082	0.16	0.26	0.36

Table 9: Maintenance fee of pollutant emission.

Type	NO_X	CO_2	CO	SO_2
Value (g/kWh)	0.6188	184.0829	0.1702	0.000928
Maintenance ($/kg)	0.250	0.00125	0.020	0.125

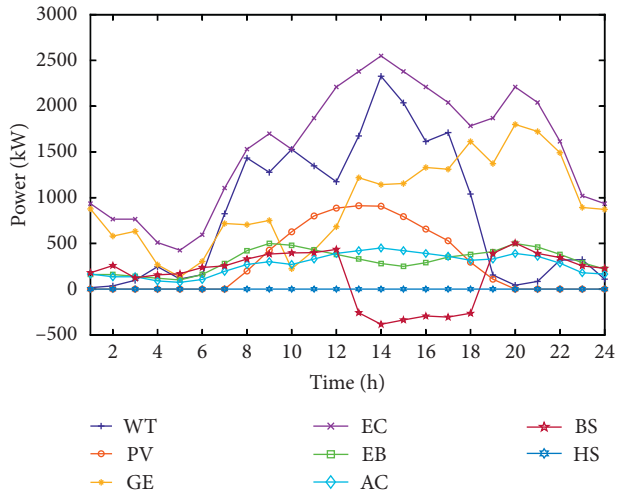

Figure 10: Real-time output value of each equipment under the priority of power load.

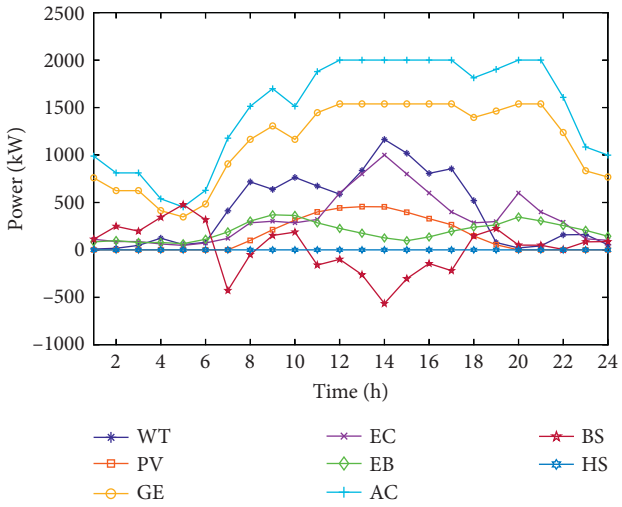

Figure 11: Real-time output value of each equipment under the priority of cooling and heating load.

Table 10: Comparison of optimization index.

	System loss ($\times 10^{-3}$)	Voltage deviation
Before optimization	7.495	0.358
After optimization final	0.283~5.225	0.012~0.324
Optimal solution	3.642	0.208

Table 11: Comparison of optimization index.

	C_{total}($)	EM_{plt}($)
Without optimization	1523.06	272.42
Priority of power load	1380.38	215.75
Priority of cooling and heating load	1267.31	264.51

thermal load priority operation mode is used, the total operation cost of the system is reduced by 16.79% and the pollutant emission treatment cost is reduced by 2.90%. Therefore, the control strategy effectively improves the operation conditions of the system, ensures the stability and economic benefits of the system, and improves the environmental protection benefits.

7. Conclusion

In this paper, a real-time optimal control strategy of multienergy complementary microgrid system based on double-layer nondominated sorting genetic algorithm can effectively solve the problems of low efficiency and poor energy management of multienergy input and multienergy output systems. This strategy optimizes the multienergy complementary microgrid system in real time and distributes the output of each energy supply terminal reasonably. According to the load demand and operation mode of the system, the first layer of the double-layer operation strategy calculates the power required by each node of the microgrid system to reduce the system loss and the second layer calculates the output of each equipment by using nondominated sorting genetic algorithm with various energy values calculated in the first layer as constraint conditions, considering the operation characteristics of various equipment and aiming at economy and environmental protection.

This paper firstly introduces two different operation modes of multienergy complementary microgrid system, nondominated sorting genetic algorithm, power load priority, and cooling and thermal load priority. Secondly, the model of typical equipment in the system is established, and then the specific expression form of double-layer optimization algorithm in the multienergy complementary microgrid system is studied. Finally, the control strategy for multienergy complementary microgrid system is applied into a certain area; the results show that the control strategy can effectively reduce the network loss, improve the system voltage, reduce the total cost of system operation, and increase the environmental benefits of the system.

Data Availability

The data used to support the findings of this study are included within the article.

Conflicts of Interest

The authors declare no conflicts of interest.

Acknowledgments

This work was supported by the National Key R&D Program of China No. 2018YFB0905101.

References

[1] Yu Han, Ke Peng, J. Wang, b. Xu et al., "Research status and prospect of key technologies for coordinated control of multi-energy synergic integrated energy systems," *Electric Power Construction*, vol. 39, no. 12, pp. 81–87, 2018.

[2] J. L. Bernal-Agustín, R. Dufo-López, and D. M. Rivas-Ascaso, "Design of isolated hybrid systems minimizing costs and

pollutant emissions," *Renewable Energy*, vol. 31, no. 14, pp. 2227–2244, 2006.

[3] D. Abbes et al., "Life cycle cost, embodied energy and loss of power supply probability for the optimal design of hybrid power systems," *Mathematics and Computers in Simulation*, vol. 98, no. 1, pp. 46–62, 2014.

[4] S. Diaf et al., "Design and techno-economical optimization for hybrid PV/wind system under various meteorological conditions," *Applied Energy*, vol. 85, no. 10, pp. 968–987, 2008.

[5] M. Ding et al., "Operation optimization for microgrids under centralized control," in *Proceedings of the 2010 2nd IEEE International Symposium on Power Electronics for Distributed Generation Systems (PEDG)*, Hefei, China, June 2010.

[6] J. Aghaei and M.-I. Alizadeh, "Multi-objective self-scheduling of CHP (combined heat and power)-based microgrids considering demand response programs and ESSs (energy storage systems)," *Energy*, vol. 55, pp. 1044–1054, 2013.

[7] N. I. Nwulu and X. Xia, "Optimal dispatch for a microgrid incorporating renewables and demand response," *Renewable Energy*, vol. 101, pp. 16–28, 2017.

[8] M. Mou, Da. Lin, Y. Zhou et al., "An optimal allocation strategy for multi-energy networks based on double-layer non-dominated sorting genetic algorithms," *Complexity*, vol. 2019, Article ID 5367403, 2019.

[9] Z. Yang, K. Li, and A. Foley, "Computational scheduling methods for integrating plug-in electric vehicles with power systems: a review," *Renewable and Sustainable Energy Reviews*, vol. 51, pp. 396–416, 2015.

[10] B. S. Borowy and Z. M. Salameh, "Methodology for optimally sizing the combination of a battery bank and PV array in A wind/PV hybrid system," *IEEE Transactions on Energy Conversion*, vol. 11, no. 2, pp. 367–375, 1996.

[11] Z. Chen, Y. Liu, Z. Yang, X. Fu, J. Tan, and X. Yang, "An enhanced teaching-learning-based optimization algorithm with self-adaptive and learning operators and its search bias towards origin," *Swarm and Evolutionary Computation*, vol. 60, Article ID 100766, 2020.

[12] R. Wang, "Research on multi-objective optimization design and coordinated control of distributed generation and microgrid," Shandong University, Jinan, China, 2013.

[13] W. Khattam, K. Bhattacharya, Y. Hegazy et al., "Optimal investment planning for distributed generation in a competitive electricity market," *IEEE Transaction on Power System*, vol. 19, no. 3, pp. 1674–1684, 2004.

[14] D. Liu, K. C. Tan, C. K. Goh, and W. K. Ho, "A multiobjective memetic algorithm based on particle swarm optimization," *IEEE Transactions on Systems, Man and Cybernetics, Part B (Cybernetics)*, vol. 37, no. 1, pp. 42–50, 2007.

[15] Z. Yu, R. Hao, and Q. Ai, "Interaction mechanism of industrial park based on multi-energy complementation," *Electric Power Automation Equipment*, vol. 37, no. 6, pp. 260–267, 2017.

[16] F. Cheng, L. Qu, W. Qiao, C. Wei, and L. Hao, "Fault diagnosis of wind turbine gearboxes based on DFIG stator current envelope analysis," *IEEE Transactions on Sustainable Energy*, vol. 10, no. 3, pp. 1044–1053, 2019.

[17] Z. Yang, M. Mourshed, K. Liu, X. Xu, and S. Feng, "A novel competitive swarm optimized RBF neural network model for short-term solar power generation forecasting," *Neurocomputing*, vol. 397, pp. 415–421, 2020.

[18] X. Xu, H. Jia, H.-D. Chiang, and D. Wang, "Dynamic modeling and interaction of hybrid natural gas and electricity supply system in microgrid," *IEEE Transactions on Power Systems*, vol. 30, no. 3, pp. 1212–1221, 2015.

[19] C. Wei, M. Benosman, and T. Kim, "Online parameter identification for state of power prediction of lithium-ion batteries in electric vehicles using extremum seeking," *International Journal of Control, Automation and Systems*, vol. 17, no. 11, pp. 2906–2916, 2019.

[20] M. Gandomkar, M. Vakilian, and M. Ehsan, "A genetic-based tabu search algorithm for optimal DG allocation in distribution networks," *Electric Power Components and Systems*, vol. 33, no. 12, pp. 1351–1362, 2005.

[21] C. L. T. Borges and D. M. Falcão, "Optimal distributed generation allocation for reliability, losses, and voltage improvement," *International Journal of Electrical Power & Energy Systems*, vol. 28, no. 6, pp. 413–420, 2006.

[22] A. Kazemi and M. Sadeghi, "Distributed generation allocation for loss reduction and voltage improvement," in *Proceedings of the IEEE Conference on Power and Energy Engeering*, pp. 518–524, Wuhan, China, March 2009.

[23] A. Chowdhury, K. Sudhir, and O. Don, "Reliability modeling of distributed generation in conventional distribution systems planning and analysis," *IEEE Transactions on Industry Applications*, vol. 39, no. 5, pp. 1493–1498, 2003.

[24] C. Wang, B. Hong, L. Guo et al., "A general modeling for optimal dispatch of combined cooling, heating and power microgrid," *Proceedings of the CSEE*, vol. 33, no. 31, pp. 26–33, 2013.

[25] A. C. Chapman, G. Verbic, and D. J. Hill, "Algorithmic and strategic aspects to integrating demand-side aggregation and energy management methods," *IEEE Transactions on Smart Grid*, vol. 7, pp. 1–13, 2016.

[26] D. Singh and K. Verma, "Multiobjective optimization for DG planning with load models," *IEEE Transactions on Power Systems*, vol. 24, no. 1, pp. 427–436, 2009.

[27] M. A. Abido, "Environmental/economic power dispatch using multiobjective evolutionary algorithms," *IEEE Transactions on Power Systems*, vol. 18, no. 4, pp. 1529–1537, 2003.